

# Revealing the Nature of Active Oxygen Species and Reaction Mechanism of Ethylene Epoxidation by Supported Ag/ $\alpha$ -Al<sub>2</sub>O<sub>3</sub> Catalysts

Tiancheng Pu, Adhika Setiawan, Alexandre C. Foucher, Mingyu Guo, Jih-Mirn Jehng, Minghui Zhu, Michael E. Ford, Eric A. Stach,\* Srinivas Rangarajan,\* and Israel E. Wachs\*



Cite This: *ACS Catal.* 2024, 14, 406–417



Read Online

ACCESS |



Metrics & More



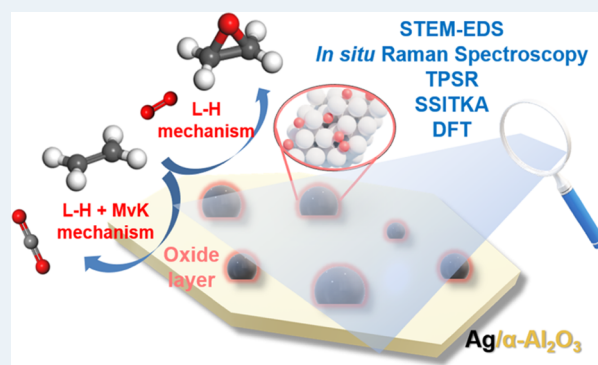
Article Recommendations



Supporting Information

**ABSTRACT:** The oxygen species on Ag catalysts and reaction mechanisms for ethylene epoxidation and ethylene combustion continue to be debated in the literature despite decades of investigation. Fundamental details of ethylene oxidation by supported Ag/ $\alpha$ -Al<sub>2</sub>O<sub>3</sub> catalysts were revealed with the application of high-angle annular dark-field-scanning transmission electron microscopy-energy-dispersive X-ray spectroscopy (HAADF-STEM-EDS), *in situ* techniques (Raman, UV-vis, X-ray diffraction (XRD), HS-LEIS), chemical probes (C<sub>2</sub>H<sub>4</sub>-TPSR and C<sub>2</sub>H<sub>4</sub> + O<sub>2</sub>-TPSR), and steady-state ethylene oxidation and SSITKA (<sup>16</sup>O<sub>2</sub> → <sup>18</sup>O<sub>2</sub> switch) studies. The Ag nanoparticles are found to carry a considerable amount of oxygen after the reaction. Density functional theory (DFT) calculations indicate the oxidative reconstructed p(4 × 4)-O-Ag(111) surface is stable relative to metallic Ag(111) under the relevant reaction environment. Multiple configurations of reactive oxygen species are present, and their relevant concentrations depend on treatment conditions. Selective ethylene oxidation to EO proceeds with surface Ag<sub>4</sub>-O<sub>2</sub>\* species (dioxygen species occupying an oxygen site on a p(4 × 4)-O-Ag(111) surface) only present after strong oxidation of Ag. These experimental findings are strongly supported by the associated DFT calculations. Ethylene epoxidation proceeds via a Langmuir–Hinshelwood mechanism, and ethylene combustion proceeds via combined Langmuir–Hinshelwood (predominant) and Mars–van Krevelen (minor) mechanisms.

**KEYWORDS:** oxidation, ethylene, silver, supported catalyst, electron microscopy, Raman, isotope, DFT



## 1. INTRODUCTION

Catalytic ethylene (C<sub>2</sub>=) epoxidation for the production of ethylene oxide (EO) is one of the largest volume reactions in the chemical industry.<sup>1</sup> The global market for EO is estimated at U.S. \$45 Billion in 2020 and is expected to reach U.S. \$65 Billion by 2027 because of the increasing demand for ethylene glycol automotive antifreeze.<sup>2</sup> An unpromoted, supported Ag/ $\alpha$ -Al<sub>2</sub>O<sub>3</sub> catalyst typically achieves an EO selectivity of ~50%.<sup>3,4</sup> With the addition of Cl, Cs, Re, and other elements such as Mo, Mn, and S as promoters, the EO selectivity can be dramatically increased to ~90%.<sup>5,6</sup> The CO<sub>2</sub> produced from unselective ethylene combustion is estimated at 9.3 million metric tons per year, which accounts for 0.03% of annual CO<sub>2</sub> emissions.<sup>7</sup> Elucidation of the oxygen species involved in the selective and unselective reaction pathways during ethylene oxidation is critical for the rational design of highly selective EO catalysts for improving process economics and mitigating CO<sub>2</sub> emissions.

Over the past 50 years, the nature of the surface oxygen species on Ag catalysts for selective ethylene epoxidation and

nonselective total combustion has been extensively debated. Barteau et al. performed temperature-programmed reaction (TPR) spectroscopy studies with a mildly oxidized single-crystal Ag(110) surface (600 L of O<sub>2</sub> at -103 °C) and co-adsorbed ethylene (60 L at -103 °C) but only observed formation of CO<sub>2</sub> and H<sub>2</sub>O under the ultrahigh vacuum (UHV) conditions.<sup>8</sup> Owing to the fact that ethylene desorbs from the Ag(110) crystal surface at a lower temperature than the CO<sub>2</sub> and H<sub>2</sub>O products, Barteau et al. surmised that the CO<sub>2</sub> and H<sub>2</sub>O result from oxidation of other reactive hydrocarbon impurities (e.g., CH≡CH) present in the ethylene gas. Campbell et al. also employed TPR spectroscopy of C<sub>2</sub>= over a mildly pre-oxidized single-crystal Ag(110)

**Received:** September 13, 2023

**Revised:** December 6, 2023

**Accepted:** December 6, 2023

**Published:** December 19, 2023



containing surface O\* atomic species ( $3 \times 10^{-4}$  Torr of O<sub>2</sub> at 217 °C) with co-adsorbed ethylene (1–10 Torr at 27–327 °C).<sup>9</sup> Only the CO<sub>2</sub> and H<sub>2</sub>O reaction products were also observed without formation of ethylene oxide (EO) under UHV conditions. This observation led Campbell et al. to conclude that surface atomic oxygen species contribute to nonselective oxidation of ethylene to CO<sub>2</sub> and H<sub>2</sub>O.

Bukhtiyarov et al.,<sup>10</sup> Grant et al.,<sup>11</sup> and Waugh et al.<sup>12,13</sup> applied stronger oxidizing environments to polycrystalline Ag foil, Ag(111) single crystal, and a supported Ag/ $\alpha$ -Al<sub>2</sub>O<sub>3</sub> catalyst, respectively, and observed formation of EO, CO<sub>2</sub>, and H<sub>2</sub>O as reaction products during TPR. Bukhtiyarov et al. initially oxidized the surface of a metallic Ag foil with a C<sub>2</sub>H<sub>4</sub> + <sup>16</sup>O<sub>2</sub> reaction mixture ( $T = 197$  °C and  $P = 100$  Pa) to form surface <sup>16</sup>O-containing oxygen (assigned to electrophilic oxygen from XPS B.E. = 530.6 eV).<sup>10</sup> The Ag surface was then exposed to an <sup>18</sup>O<sub>2</sub> isotope treatment ( $T = 197$  °C and  $P = 1$  Pa), and the surface <sup>18</sup>O-containing oxygen was assigned to nucleophilic oxygen from XPS (B.E. = 528.4 eV). Subsequently, ethylene was adsorbed ( $P = 10$  Pa for 10 min) onto the oxidized Ag surface at room temperature, and TPR of the adsorbed ethylene and isotopically labeled oxygen species were performed under UHV conditions. It was found that only surface <sup>16</sup>O participates in EO (C<sub>2</sub>H<sub>4</sub><sup>16</sup>O) formation while both surface <sup>16</sup>O and <sup>18</sup>O participate in CO<sub>2</sub> (C<sup>16</sup>O<sub>2</sub> and C<sup>18</sup>O<sub>2</sub>) production (formation of C<sup>18</sup>O<sup>16</sup>O was not monitored).<sup>10</sup> Grant et al. dosed the Ag(111) surface with  $5 \times 10^6$  L O<sub>2</sub> and then exposed the strongly oxidized Ag surface to  $9 \times 10^6$  L C<sub>2</sub>H<sub>4</sub> at 50 Torr and 27 °C and found that both selective (EO formation) and nonselective (CO<sub>2</sub> + H<sub>2</sub>O formation) ethylene oxidation took place during TPR.<sup>11</sup> Atkins et al. also observed production of both EO and CO<sub>2</sub> during C<sub>2</sub><sup>=</sup>-TPR (2% C<sub>2</sub><sup>=</sup>,  $P = 101$  kPa, flow of 25 cm<sup>3</sup> min<sup>-1</sup>) from a strongly pre-oxidized Ag/ $\alpha$ -Al<sub>2</sub>O<sub>3</sub> catalyst (O<sub>2</sub> ( $P = 101$  kPa) for 1 h at 500 °C).<sup>12</sup> The above-reported TPR spectroscopy studies are compared in Figure S1. For the studies observing EO formation, the EO and CO<sub>2</sub> formation coincided at  $\sim 100$  °C, suggesting that both products may come from a common surface reaction intermediate at mild temperatures ( $\sim 100$  °C). Furthermore, it appears that EO formation requires an Ag surface with higher surface oxygen coverage (Bukhtiyarov et al.,<sup>10</sup> Grant et al.,<sup>11</sup> and Waugh et al.<sup>12,13</sup>) that has also been elucidated by *ab initio* calculations of the Ag(111) surface with different surface O\* coverage<sup>14</sup> and an Ag<sub>x</sub>O cluster model.<sup>15</sup> The lack of *in situ/operando* spectroscopic information associated with previous TPR studies has hampered the establishment of corresponding structure–activity/selectivity relationships between the nature of oxygen species on/in Ag and the selective (EO) and nonselective (CO<sub>2</sub> and H<sub>2</sub>O) ethylene oxidation products.

The nature of oxygen species on/in Ag was addressed with surface-enhanced Raman spectroscopy (SERS) in several studies.<sup>16</sup> Pettenkofer et al. examined the nature of oxygen on freshly prepared silver films at 120 K and observed multiple Raman bands after exposure to 2 L of molecular O<sub>2</sub> at  $1 \times 10^{-6}$  Torr.<sup>17</sup> The band assignments were made by comparison with matrix isolated Ag–O<sub>x</sub> references: 1053 cm<sup>-1</sup> (superoxide Ag–O<sub>2</sub><sup>-</sup>), 697 cm<sup>-1</sup> (peroxide Ag–O<sub>2</sub><sup>2-</sup>), 300–500 cm<sup>-1</sup> (multiple atomic Ag–O species), and Raman bands at 815 and 1286 cm<sup>-1</sup> (unassigned, but must arise from Ag–O<sub>2</sub> species because of the high bond order). The decomposition of the Ag<sub>2</sub>O<sub>8</sub>NO<sub>3</sub> compound at elevated temperatures was investigated with *in situ* Raman spectroscopy by Pettinger et al. and observed

Raman vibrations at 410 cm<sup>-1</sup> (assigned to lattice atomic oxygen of AgO),  $\sim 630$  cm<sup>-1</sup> (assigned to subsurface atomic O <sub>$\beta$</sub>  species), and  $\sim 800$  cm<sup>-1</sup> (assigned to strongly chemisorbed surface atomic O <sub>$\gamma$</sub>  species).<sup>18</sup> Recently, several studies combined *in situ* Raman spectroscopy and density functional theory (DFT) calculations to more rigorously assign the oxygen vibrations of unsupported Ag catalysts in oxidizing and ethylene oxidation reaction environments.<sup>19,20</sup> Liu et al. detected Raman vibrations at  $\sim 810$ – $840$  cm<sup>-1</sup> on unsupported Ag powder catalysts that were assigned to surface dioxygen species based on DFT calculations.<sup>21</sup> Pu et al. also reported that during ethylene epoxidation by unsupported Ag powder catalysts, Raman vibrations are present at 691–721 and 840 cm<sup>-1</sup> that correspond to Ag<sub>4</sub>–O<sub>2</sub> species with the aid of DFT calculations.<sup>20</sup> These two studies, along with recent surface science analyses, probed the various oxygen species on partially reconstructed Ag configurations with oxygen atoms integrated as part of the new surface model, such as the p(4 × 4) oxidic reconstruction of the Ag(111) surface.<sup>22,23</sup> Tang et al. employed DFT to calculate the oxygen vibrations for supported Ag/Al<sub>2</sub>O<sub>3</sub> (sapphire) of atomic oxygen (Ag<sub>n</sub>–O<sub>surf</sub>), hybrid dioxygen (Ag–O<sub>sur</sub>–O<sub>sub</sub>), and molecularly adsorbed O<sub>2</sub> species on an oxidized Ag surface that yielded vibrations at 240–500, 600–810, and 870–1150 cm<sup>-1</sup>, respectively.<sup>19</sup> This study particularly highlighted how different local structures of surface adsorbed and subsurface oxygen prephase reconstruction could result in different oxygen species with a 200 cm<sup>-1</sup> spread in vibrational frequencies. It should be noted that, although several studies have reported on the thermodynamic stability of these oxidic reconstructions of Ag, much less is understood regarding the mechanism and kinetics behind the phase transition between the metallic Ag surface into its oxidized variants.<sup>21,24</sup> Given the multiple oxygen species present on/in oxidized Ag particles, it is critical to employ molecular spectroscopic methods to be able to distinguish among the various oxygen species. When non-molecular spectroscopic methods are applied, the signals will be dominated by the most abundant oxygen species and also be volume averaged when the analysis method involves sampling multiple layers (e.g., XAS, XPS, Auger, UPS, etc.).<sup>25</sup>

Many attempts have been made to determine the ethylene oxidation reaction mechanism on Ag/Al<sub>2</sub>O<sub>3</sub> by fitting rate expressions to steady-state experimental kinetics data; however, this has led to contradicting conclusions. For example, both one site Eley–Rideal<sup>26–28</sup> (E–R, recently also referred as Langmuir–Rideal (L–R))<sup>29</sup> and dual site Langmuir–Hinshelwood (L–H) reaction mechanisms have been postulated.<sup>30–32</sup> It has also been proposed that selective ethylene epoxidation proceeds through the E–R mechanism whereas the total combustion follows the L–H mechanism.<sup>33</sup> Furthermore, the formation of selective and nonselective ethylene oxidation products under anaerobic conditions from the previous TPR studies with pre-oxidized Ag surfaces clearly suggests a possible limited contribution of the Mars–van–Krevelen (MvK) reaction mechanism that has not been systematically investigated.<sup>33</sup>

Herein, a series of *in situ* spectroscopic and microscopic techniques are applied to provide direct information about the nature and reactivity of various oxygen species on/in supported Ag particles for selective and nonselective ethylene oxidation reaction mechanisms over the supported Ag/ $\alpha$ -Al<sub>2</sub>O<sub>3</sub> catalyst. The collective results support the conclusions that ethylene epoxidation proceeds through a L–H mechanism

with surface dioxygen species ( $\text{Ag}_4\text{-O}_2^*$ ) being the more selective oxygen species responsible, and ethylene combustion proceeds through L–H and MvK mechanisms with surface and subsurface atomic oxygen ( $\text{O}^*$ ) species. Furthermore, the combination of the various techniques brought together to address this catalyst study serve as a powerful toolbox for the elucidation of structure–activity/selectivity relationships for other heterogeneous catalyst systems.

## 2. METHODS

**2.1. Materials.** The  $\alpha\text{-Al}_2\text{O}_3$  support was purchased from CeramTec. Silver oxalate ( $\geq 99\%$ ) was prepared from  $\text{AgNO}_3$  (Sigma,  $\geq 99\%$ ) and aqueous oxalic acid (Sigma-Aldrich,  $\geq 99\%$ ) solution. Ethylene diamine was purchased from JT Baker ( $\geq 98\%$ ). The gas supplies (Ar, 40% and 5%  $\text{O}_2/\text{He}$ , 25% and 5%  $\text{C}_2\text{H}_4(\text{C}_2^=)/\text{He}$ , 1%  $\text{O}_2/\text{He}$ ) for high-sensitivity-low-energy ion scattering (HS-LEIS), temperature-programmed surface reaction (TPSR), and steady-state ethylene oxidation experiments were purchased from Praxair. The  $\text{C}^{18}\text{O}_2$  for *in situ* Raman spectroscopy during  $\text{C}^{18}\text{O}_2$  exchange as well as for HS-LEIS was supplied by Sigma-Aldrich (97%  $^{18}\text{O}$  atomic purity, chemical purity > 99%). The 1%  $^{18}\text{O}_2/\text{Ar}$  used in the steady-state isotopic transient kinetic analysis (SSITKA) experiment was purchased from Isotec (98%  $^{18}\text{O}$  atomic purity). The gas supplies (Ar, He, 5%  $\text{O}_2/\text{He}$ , 40%  $\text{O}_2/\text{He}$ , and 5%  $\text{C}_2\text{H}_4/\text{Ar}$ ) for *in situ* spectroscopies were purchased from Air Liquid. Bulk Ag powder was obtained from Handy & Harman (99.9999%, 30–60 mesh).

**2.2. Catalyst Synthesis.** The  $\text{Ag}/\alpha\text{-Al}_2\text{O}_3$  catalyst with Ag loading of 15 wt % was prepared with the standard incipient-wetness impregnation method by using silver oxalate as the precursor. The Ag complex solution was first prepared by mixing silver oxalate, ethylene diamine, and deionized water at a mass ratio of 1:0.5:0.5. The desired amount of solution was mixed with  $\alpha\text{-Al}_2\text{O}_3$  support and stirred for 30 min. The mixture was allowed to dry at 90 °C overnight before being calcined at 450 °C in  $\text{N}_2$  for 45 min. For the fixed-bed steady-state kinetic studies, the catalysts were pelletized and sieved between 40–60 mesh.

**2.3. Scanning Transmission Electron Microscopy (STEM).** STEM characterization was performed on a JEOL JEM-F200 STEM operated at 200 kV. The powdered supported  $\text{Ag}/\alpha\text{-Al}_2\text{O}_3$  catalysts were dispersed in 2-propanol and then deposited on lacey carbon films on copper grids. Images of fresh catalysts were taken from the as-prepared samples. The spent catalyst used for imaging was taken from the steady-state reactor after 24 h of ethylene oxidation reaction. After reaction, the catalyst was cooled down to room temperature under the reaction mixture followed by flowing Ar for 30 min.

**2.4. *In Situ* Raman Spectroscopy of Oxidized Ag during  $\text{C}^{18}\text{O}_2$  Exchange.** Raman spectra were obtained with visible (532 nm) laser excitation on a single-stage Horiba–Jobin Yvon Laboratory Ram-HR Raman spectrometer with a confocal microscope (Olympus BX-30), notch filter (Kaiser Super Notch), and a 900 grooves/mm grating. The visible laser excitation was generated with a Nd:YAG double diode-pumped laser (Coherent Compass 315M-150, output power of 150 mW with sample power 10 mW). The scattered photons were directed into a single monochromator and focused onto a UV-sensitive LN<sub>2</sub>-cooled CCD detector (Horiba–Jobin Yvon CCD-3000 V) with a spectral resolution of  $\sim 1\text{ cm}^{-1}$  for the given parameters. The Raman spectra were

collected above  $200\text{ cm}^{-1}$ . The laser was calibrated before each experiment using the  $520.7\text{ cm}^{-1}$  peak of a silicone standard. Gas flow rates were adjusted by using mass flow controllers (Brooks, Model S850E). For each experiment, the catalyst was loaded as a loose powder ( $\sim 20\text{ mg}$ ) into an *in situ* environmental cell (Harrick, HVC-DR2 with a  $\text{CaF}_2$  window). The  $\text{Ag}/\alpha\text{-Al}_2\text{O}_3$  catalyst was first oxidatively dehydrated in flowing 10%  $\text{O}_2/\text{Ar}$  at 50 sccm and 300 °C. The catalyst was cooled to 25 °C and then flushed with Ar to remove  $\text{O}_2$ . Temperature-programmed  $\text{C}^{18}\text{O}_2$  exchange is then performed at 25–200 °C at 10 sccm.

**2.5. Temperature-Programmed Surface Reaction (TPSR) Spectroscopy of Gas-Phase Ethylene with the Pre-Oxidized Catalyst Surface.** TPSR experiments were performed on an Altamira Instruments (AMI 200) system. The catalysts were loaded in a U-tube reactor. The temperature was measured by a thermocouple touching the top of the catalyst bed. The outlet gases were analyzed by an online mass spectrometer (Dymaxion Dycor, DME400MS). For mildly oxidized  $\text{Ag}/\alpha\text{-Al}_2\text{O}_3$ , the catalyst surface was oxidized with 5%  $\text{O}_2/\text{He}$  at 175 °C for 30 min. For strongly oxidized  $\text{Ag}/\alpha\text{-Al}_2\text{O}_3$ , the catalyst surface was oxidized with 40%  $\text{O}_2/\text{He}$  at 250 °C for 30 min.  $\text{C}_2^+ + \text{O}_2$ -TPSR was performed over the strongly oxidized  $\text{Ag}/\alpha\text{-Al}_2\text{O}_3$  with 10%  $\text{C}_2^+$  and 4%  $\text{O}_2$  balanced by He from 30 to 300 °C at a ramping rate of 10 °C/min. Temperature-programmed reactions of ethylene with the supported  $\text{Ag}/\alpha\text{-Al}_2\text{O}_3$  catalysts were performed from 50 to 500 °C in flowing 5%  $\text{C}_2\text{H}_4/\text{He}$  (Praxair, Purity 99.9 vol %) with a ramping rate of 10 °C/min. The reaction products were determined with online MS.

**2.6. *In Situ* Raman Spectroscopy during TPSR of  $\text{C}_2^+$  with Oxidized  $\text{Ag}/\alpha\text{-Al}_2\text{O}_3$ .** The *in situ* Raman spectra of the  $\text{Ag}/\alpha\text{-Al}_2\text{O}_3$  catalysts were obtained on different sample spots irradiated by a visible 514.5 nm  $\text{Ar}^+$  laser. A plate of single-crystal silicon was used for the instrumental correction of the Raman peak at  $520.7\text{ cm}^{-1}$ . The 200  $\mu\text{m}$  confocal hole was selected for all measurements. The attenuator was used for the tests to avoid signal overflow and sample degradation. The maximum intensity irradiating to the samples was 4 mW, and no damage to the samples was observed. The exposure time was set to 90 s for each spectrum. The backscattered light was detected by a deep-depleted thermoelectrically cooled CCD array detector ( $1024 \times 256$  pixels, 26  $\mu\text{m}$  in size). Twenty mg of  $\text{Ag}/\alpha\text{-Al}_2\text{O}_3$  powder and 50 sccm of 5%  $\text{C}_2^+/\text{He}$  flow are used in each experiment. The procedures of the different oxidation treatments and subsequent Raman/TPSR investigations are demonstrated in Scheme S1.

**2.7. *In Situ* Raman Spectroscopy of Ethylene Adsorption on Oxidized Ag Surface of Supported  $\text{Ag}/\alpha\text{-Al}_2\text{O}_3$ .** The low temperature *in situ* Raman was performed by using Linkam THMS600 heating/cooling stage with a temperature range from  $< -195$  to 600 °C (cooling using LNP96 cooling pump). The *in situ* Raman spectra were recorded in the following steps: (1) The sample was first dehydrated at 300 °C for 1 h under flowing 10%  $\text{O}_2/\text{Ar}$  mixed gas and (2) cooled to 25 °C in the same oxygen environment. (3) A He carrier gas was introduced into the cell to flush out the oxygen molecules for 30 min at 25 °C. (4) The sample was further cooled to 0 °C under He environment, then (5) switched to 20%  $\text{C}_2\text{H}_4/\text{He}$  reactant gas to adsorb for 55 min, then (6) flushed with He gas for 30 min. (7) A heating profile was started from 0 to 50 °C with a 1 °C/min ramping rate.

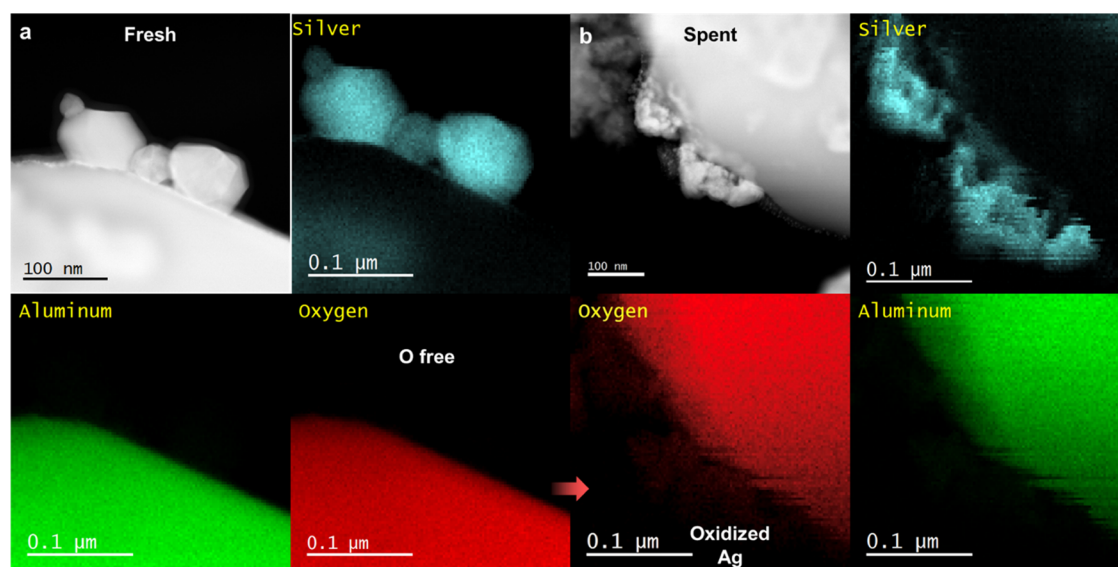


**Figure 1.** HAADF-STEM images and EDS mappings of (a) fresh Ag/ $\alpha$ -Al<sub>2</sub>O<sub>3</sub> catalyst (calcined at 450 °C in N<sub>2</sub>) and (b) spent Ag/ $\alpha$ -Al<sub>2</sub>O<sub>3</sub> catalyst after exposure to steady-state ethylene oxidation at 225 °C (25% C<sub>2</sub>H<sub>4</sub>, 7% O<sub>2</sub>, and 2% CO<sub>2</sub> balanced by He) for 24 h.

**2.8. Steady-State Ethylene Oxidation with Isotopic <sup>16</sup>O<sub>2</sub> → <sup>18</sup>O<sub>2</sub> Switch.** The steady-state isotopic transient kinetic analysis (SSITKA) experiment was performed on an Altamira Instruments (AMI-200) system. In a typical experiment, 0.25 g of catalyst was placed in the U-tube reactor, which was held in place with quartz wool, and the WHSV was adjusted to 6000 mL/(gcat·h). The catalyst was first oxidatively dehydrated with 5% O<sub>2</sub>/He at 300 °C for 10 min. Steady-state ethylene oxidation was then performed at 225 °C to condition the catalyst with a mixture of 1.2% C<sub>2</sub>H<sub>4</sub> and 3000 ppm of O<sub>2</sub> with a balance of Ar at a total flow rate of 25 sccm for 50 min. The 3000 ppm <sup>16</sup>O<sub>2</sub>/Ar flow was then replaced by 3000 ppm <sup>18</sup>O<sub>2</sub>/Ar (Isotec) during the steady-state ethylene oxidation reaction, and the oxygen isotope products of EO and CO<sub>2</sub> were followed with the online mass spectrometer.

**2.9. DFT Calculations.** All DFT calculations were carried out using the Vienna Ab-initio Simulation Package (VASP) software.<sup>34–37</sup> Periodic boundary conditions are used, with each unit cell including a 10 Å vacuum above the simulated surface. Metallic silver facets ((111), (110), (100)) are simulated using four layers of a 3 × 3 unit cell, while oxidic reconstructed silver facets (p(4 × 4)–O–Ag(111)) are simulated using four layers of a 4 × 4 unit cell. All calculations are done using the Projector augmented wave (PAW) potential with generalized gradient approximation (GGA) along with the Perdew–Burke–Ernzerhof (PBE) exchange–correlation functional with a dDsC dispersion correction. An energy cutoff of 500 eV with an SCF convergence criterion of 10<sup>−6</sup> eV and a force-convergence criterion of 0.02 eV/Å is used. Methfessel–Paxton smearing with a spread of 0.1 eV and a Monkhorst–Pack 5 × 5 × 1 K-point sampling is used.

### 3. RESULTS AND DISCUSSION

#### 3.1. Morphology of $\alpha$ -Al<sub>2</sub>O<sub>3</sub>–Supported Ag Particles.

To give an illustration of the morphology of the Ag particles before and after exposure to the ethylene oxidation reaction environment, *ex situ* high-angle annular dark-field scanning transmission electron microscopy (HAADF-STEM) with energy dispersive spectroscopy (EDS) mapping images of the

fresh and spent supported Ag/ $\alpha$ -Al<sub>2</sub>O<sub>3</sub> catalysts are compared in Figure 1a,b, respectively. For the fresh catalyst calcined at 450 °C in N<sub>2</sub>, the Ag particles appear to be well-crystallized with sharp corners and straight edges. After the fresh Ag/ $\alpha$ -Al<sub>2</sub>O<sub>3</sub> catalyst is exposed to 24 h of ethylene oxidation at 225 °C, significant morphologic variations can be observed compared to the fresh catalyst. The Ag particles of the spent catalyst are not as well-crystallized, lack sharp corners and straight edges, and possess pores. Particle size analysis indicates that the Ag nanoparticles for the fresh supported Ag/ $\alpha$ -Al<sub>2</sub>O<sub>3</sub> catalyst are concentrated in the 30–70 nm range while they are larger and concentrated in the 60–120 nm range for the spent supported Ag/ $\alpha$ -Al<sub>2</sub>O<sub>3</sub> catalyst (Figure S2). Significant oxygen is not detected to be associated with the Ag nanoparticles of the fresh catalyst calcined in N<sub>2</sub>, but oxygen is found to be associated with the Ag nanoparticles of the spent catalyst after ethylene oxidation. Zoom in of EDS mapping of a Ag nanoparticle located on the edge of support on spent catalyst further verifies that the Ag particle also contains substantial oxygen after reaction, which is likely to concentrate at the near-surface region (Figure S3). The dramatically different morphologies of the supported Ag nanoparticles and oxygen distributions of the fresh and spent Ag/ $\alpha$ -Al<sub>2</sub>O<sub>3</sub> catalysts indicate two important findings. First, the bulk and surface of the Ag nanoparticles are dynamic since the surface area both simultaneously decreases and increases from sintering of the Ag nanoparticles and void formation, respectively, which is related to the low Tammann temperature of metallic Ag (~344 °C).<sup>38–40</sup> Second, the oxygen maps for the fresh and spent catalysts reveal that the Ag nanoparticles contain more oxygen after exposure to the ethylene oxidation reaction conditions. The absence of bulk Ag oxide phases during ethylene oxidation, as determined with *in situ* XRD (Figure S4a), indicates that crystalline Ag<sub>2</sub>O or AgO phases larger than 3 nm are not present and that the bulk phase of the supported Ag nanoparticles is predominately metallic. The corresponding *in situ* UV–vis spectra of the supported Ag/ $\alpha$ -Al<sub>2</sub>O<sub>3</sub> catalyst are presented in Figure S4b. The absorption bands located at 305 and 351 nm have previously been assigned to the 4d<sup>10</sup> to 4d<sup>9</sup>s<sup>1</sup> transition of Ag<sup>+</sup> ions and Ag<sub>n</sub><sup>δ+</sup> clusters, respectively, and the

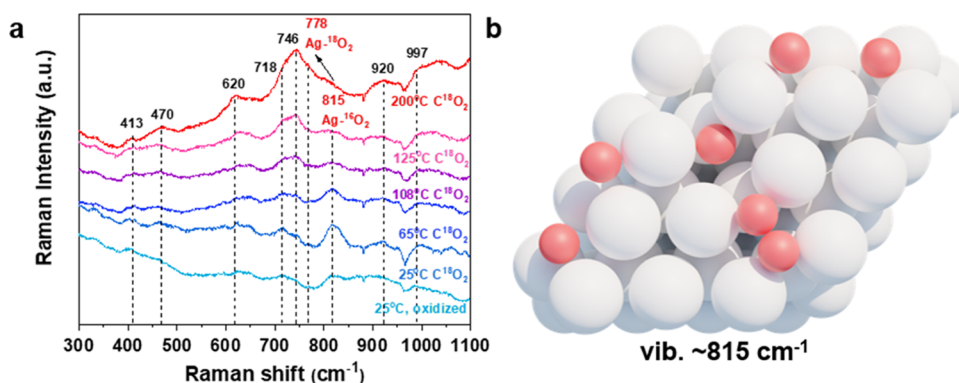


**Figure 2.** (a) *In situ* Raman spectra of oxidized supported Ag/ $\alpha$ -Al<sub>2</sub>O<sub>3</sub> catalyst Ag surface (calcined in 10% <sup>16</sup>O<sub>2</sub>/Ar at 300 °C for 1 h) and subsequently exposed to temperature-programmed C<sup>18</sup>O<sub>2</sub>-exchange from 25 to 200 °C. (b) Illustration of the corresponding Ag–O<sub>2</sub> species possessing a Raman vibration at 815 cm<sup>-1</sup>.

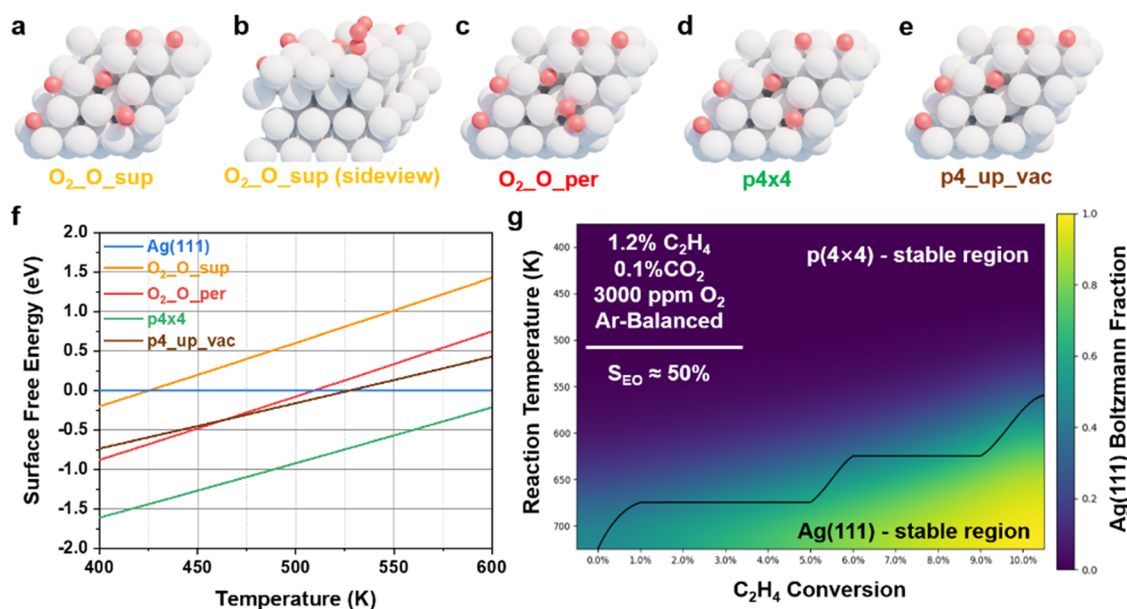


**Figure 3.** Computational insights into the various oxygen species on oxidized Ag surface. Illustration of the structures of (a) O<sub>2</sub>\_O<sub>sup</sub>, (b) side view of O<sub>2</sub>\_O<sub>sup</sub>, (c) O<sub>2</sub>\_O<sub>per</sub>, (d) p4 × 4, and (e) p4<sub>up\_vac</sub>, respectively. (f) Thermodynamic atomistic phase diagram comparing the surface free energy of different partially oxidized Ag surfaces as a function of temperature, relative to an Ag(111) slab. (g) Boltzmann fraction of metallic Ag population based on surface free energies at different temperatures and conversions under typical oxygen lean ethylene oxidation conditions.

broad band above 350 nm has been assigned to metallic Ag.<sup>41,42</sup> The above information points to the findings that supported Ag nanoparticles are not entirely metallic but partially oxidized upon exposure to an ethylene oxidation environment.

**3.2. Nature of Oxygen Species for  $\alpha$ -Al<sub>2</sub>O<sub>3</sub>–Supported Ag Catalyst.** Combined spectroscopic investigations and DFT calculations were performed to illustrate the nature of abundant oxygen species on the Ag particles. Isotopic C<sup>18</sup>O<sub>2</sub> exchange of oxidized Ag surface monitored by spectroscopies is an excellent tool to probe surface oxygen species owing to the fact that carbon dioxide readily undergoes isotopic oxygen exchange with only surface oxygen species at mild temperatures without diffusing below the surface.<sup>43–45</sup> High sensitivity-low energy ion scattering (HS-LEIS) surface analysis of the unsupported Ag confirmed that oxygen exchange takes place between gas phase C<sup>18</sup>O<sub>2</sub> and the <sup>16</sup>O-containing Ag powder (Figure S5). The unsupported Ag powder was first chosen for demonstrating the oxygen

exchange in order to avoid interactions of C<sup>18</sup>O<sub>2</sub> with the surface of the  $\alpha$ -Al<sub>2</sub>O<sub>3</sub> support and the contribution of the HS-LEIS signal from oxygen of the  $\alpha$ -Al<sub>2</sub>O<sub>3</sub> support. Note also that the oxygen is concentrated on the outermost layers (<1 nm) of the Ag particles. The temperature-dependent *operando* Raman spectra of an <sup>16</sup>O<sub>2</sub> oxidized supported Ag/ $\alpha$ -Al<sub>2</sub>O<sub>3</sub> catalyst under flowing C<sup>18</sup>O<sub>2</sub> from 25 to 200 °C are presented in Figure 2a, and the corresponding MS signals for the CO<sub>2</sub> isotopes are shown in Figure S6. Raman bands located at 413, 470, 620, 718, 815, and 920 cm<sup>-1</sup> could be resolved from the Ag nanoparticles of the oxidized Ag/ $\alpha$ -Al<sub>2</sub>O<sub>3</sub> catalyst. The Raman bands associated with the oxidized supported Ag nanoparticles are selectively enhanced by as much as  $\sim 10^{10}$  because of the surface-enhanced Raman spectroscopy (SERS) effect of Ag nanoparticles.<sup>46</sup> This is evidenced by the absence of the sharp Raman bands from the crystalline  $\alpha$ -Al<sub>2</sub>O<sub>3</sub> support (383, 421, 580, 649, and 752 cm<sup>-1</sup>, Figure S7) that are not enhanced and, thus, not observed for the Raman spectra of the supported Ag/ $\alpha$ -Al<sub>2</sub>O<sub>3</sub> catalyst (Figure 2a). The presence of

multiple Raman bands from the oxidized Ag/ $\alpha$ -Al<sub>2</sub>O<sub>3</sub> catalyst indicates that several distinct oxygen species are associated with the supported Ag nanoparticles.

Plane wave periodic DFT calculations were employed to compute the adsorption structures, binding energies, and vibrational frequencies of various oxygen species present on/in the representative p(4 × 4)-O-Ag(111) surface.<sup>20</sup> Although various stable structures of partially oxidized Ag has been reported in the literature, the p(4 × 4)-O-Ag(111) was chosen as the model catalyst for this study due to its stability relative to Ag(111) during reaction conditions, its relatively ordered structure, as well as agreement with surface science and spectroscopic studies.<sup>21–23</sup> It should be noted that the catalyst surface might contain a distribution of these differently oxidized surfaces and a small portion of Ag with metallic character, the relative population of which would depend on their surface free energies, but the p(4 × 4)-O-Ag(111) surface has been a relevant model in understanding the reaction.<sup>20</sup> Several different dioxygen species on this surface were studied and are exhibited in Figure S8, each with different positions of the dioxygen bond axis relative to the surface. These species differ not only in their configuration but also in the degree/depth of chemisorption of the dioxygen species into the trough structure on the p(4 × 4)-O-Ag(111) surface, which inherently affects their binding strength. The two most notable species are the “perpendicular” species: O<sub>2</sub>\_O<sub>sup</sub> in Figure 3a (with side view in Figure 3b) possess the weakest binding energy of −0.150 eV, and a much more stable “parallel” species: O<sub>2</sub>\_O<sub>per</sub> in Figure 3c, with the strongest binding energy of −0.829 eV (Both are DFT energy values prior to the oxygen energy corrections explained in the SI). The vibrational frequencies exhibited by these two species fall generally in agreement with previously reported results, citing the 750–800 cm<sup>−1</sup> range as corresponding to oxygen species that is incorporated closer to the subsurface level and the 1050–1100 cm<sup>−1</sup> range corresponding to a surface oxygen species with a negative charge. As an additional clarification, the structures shown in Figure 3d,e are the unmodified p(4 × 4)-O-Ag(111) surface and the same surface with one of the trough oxygen atoms removed, thereby creating an oxygen vacancy, respectively.<sup>19</sup>

To extend the discussions on the particular adsorbed dioxygen species with the Raman vibration at ~815 cm<sup>−1</sup> (Figure 2b), it should be reiterated that this band is associated with a hybrid adsorbed dioxygen species occupying the site where an atomic lattice oxygen is expected to be on a p(4 × 4)-O-Ag(111) surface as shown in Figure 3d that is distinct from the physisorption mode that is classically understood as “adsorbed O<sub>2</sub>\*” (e.g., O<sub>2</sub>/Ag(111) at low temperatures). Previous experimental and theoretical studies have reported the absence of this dioxygen species for Ag catalysts that were either metallic in nature or pre-oxidized at mild conditions.<sup>47–49</sup> In such cases, only atomic oxygen species resulting from a dissociative oxygen adsorption or a physisorbed dioxygen species (which is expected to desorb below room temperature) are shown in the spectral analyses. Our previous study confirmed this observation as well,<sup>20</sup> with milder oxidizing conditions insufficient for the generation of this newer chemisorbed dioxygen species. On the other hand, we found that a stronger oxidizing pretreatment condition (but still below the oxygen potential expected for bulk oxide stability) was necessary to generate the 815 cm<sup>−1</sup> band. Possible assigned dioxygen species that were explored via

Raman spectroscopy and DFT are listed in Table 1. Additionally, we performed thermodynamic atomistic phase

**Table 1. Assignments of Species Observed during *In Situ* Raman Spectroscopy Studies by DFT Calculations<sup>†</sup>**

raman vibration (cm <sup>−1</sup> )	assignment	DFT-calculated vibration (cm <sup>−1</sup> )
300–328	Ag <sub>3</sub> -O	335 (surface, Ag <sub>6</sub> ) 305 (subsurface, Ag <sub>6</sub> )
413–470	Ag-O	~410 (p4 × 4, down) ~ 382 (p4 × 4, up) ~ 440 (bulk Ag <sub>2</sub> O)
715–718	Ag <sub>6</sub> -O <sub>2</sub>	693 (peroxo O <sub>2</sub> , down) 760 (peroxo O <sub>2</sub> )
815–820	Ag <sub>4</sub> -O <sub>2</sub>	785 (peroxo O <sub>2</sub> , rotated)
980–990	carbonate	929 (bidentate) 968 (tridentate)
1057–1073	nitrate	1004 (bidentate) 1013 (tridentate)
1336	C=C	1317 (ethylene on p4 × 4)

<sup>†</sup>Reported frequencies for carbonates and nitrates are based on their adsorbates on a metallic Ag(111) surface and should be similar on the Ag<sub>6</sub> portion of the p(4 × 4) surface.

diagram analysis (Figure 3f), which showed that the O<sub>2</sub>\_O<sub>per</sub> species (Figure 3c) is expected to have exergonic surface free energies relative to an Ag(111) up to around 510 K. An analog of this model was also shown for the Ag<sub>2</sub>O film-like surfaces in the recent work by Paolucci et al., where a similar dioxygen species was reported to have exergonic free energies up to approximately 520 K.<sup>21</sup> An alternative perspective on the phase diagram is shown in Figure 3g, where the surface free energies at different reaction temperatures and oxygen chemical potential (which corresponds to a range of ethylene conversions, assuming a 50% EO selectivity) were used to construct a Boltzmann distribution of stable surfaces (all of the surfaces featured in Figure 3f were included in the distribution). Darker and lighter regions represent conditions where a lower and higher fraction of metallic Ag is to be expected, respectively. Above the black threshold line, the p(4 × 4)-O-Ag(111) is the thermodynamically stable surface configuration for a given oxygen chemical potential. The degree of oxidation of the outermost surface, however, might be strongly associated with the reaction environment as the typical industrial processes adopt ethylene-rich conditions with C<sub>2</sub>=/O<sub>2</sub> of 4:1.<sup>5</sup>

Experimentally, to distinguish between surface and subsurface oxygen species associated with the <sup>16</sup>O<sub>2</sub>-oxidized Ag/ $\alpha$ -Al<sub>2</sub>O<sub>3</sub> catalyst, C<sup>18</sup>O<sub>2</sub> exchange was subsequently performed (Figure 2a). It is observed that only the Raman band at 815 cm<sup>−1</sup> red shifts (from 815 to 778/745 cm<sup>−1</sup>) due to exchange with the heavier <sup>18</sup>O, indicating that this vibration is associated with surface oxygen species. The exchange was confirmed by the simultaneous formation of isotopic C<sup>16</sup>O<sub>2</sub> and C<sup>18</sup>O<sup>16</sup>O gases, with significant exchange occurring at ~200 °C (see Figure S8). Interestingly, this exchange temperature corresponds to the initial desorption of <sup>16</sup>O<sub>2</sub> from the Ag/ $\alpha$ -Al<sub>2</sub>O<sub>3</sub> catalyst (see Figure S9) that may reflect the supply of oxygen from the silver lattice at this temperature.

Simulated vibrational shifts caused by the <sup>16</sup>O–<sup>18</sup>O isotopic double exchange for dioxygen species are tabulated in Table S1 and range from 43–57 cm<sup>−1</sup>, which are in reasonable agreement with the 37–70 cm<sup>−1</sup> shift observed experimentally. Furthermore, the single isotope exchanges for the “oxygen vacancy” cases exhibited vibrational frequency shifts in the ~20 cm<sup>−1</sup> range, which is in agreement with recent computational studies.<sup>21</sup> The evolution of the normalized area of operando Raman bands during temperature-programmed C<sup>18</sup>O<sub>2</sub> ex-

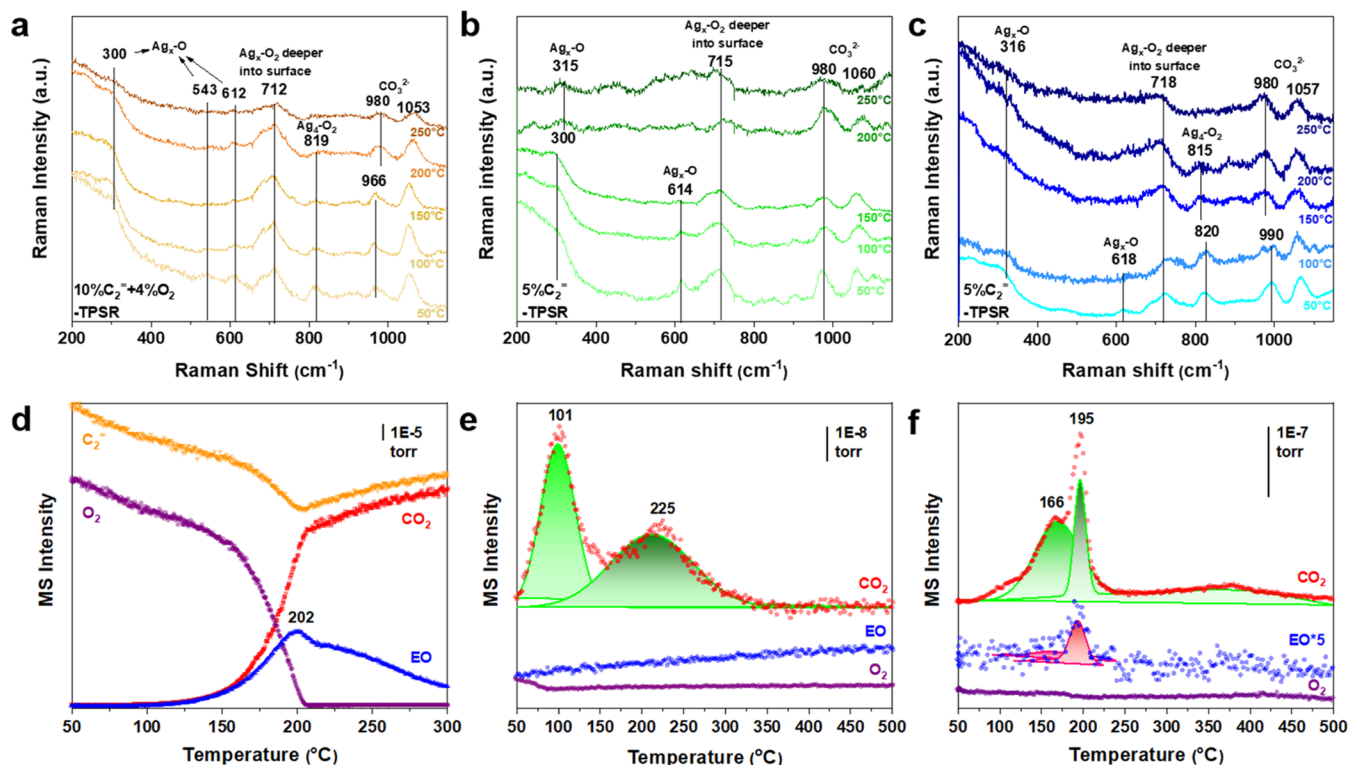


**Figure 4.** (a–c) *In situ* Raman spectra of temperature-programmed reaction (50–250 °C, spectra every 50 °C) (a) 10% C<sub>2</sub><sup>-</sup> + 4% O<sub>2</sub> over strongly oxidized Ag/α-Al<sub>2</sub>O<sub>3</sub> (40% O<sub>2</sub>, 250 °C for 30 min post dehydration), (b) 5% C<sub>2</sub><sup>-</sup> over mildly O<sub>2</sub> oxidized Ag/α-Al<sub>2</sub>O<sub>3</sub> (5% O<sub>2</sub>, 175 °C for 30 min post dehydration) and (c) 5% C<sub>2</sub><sup>-</sup> over strongly O<sub>2</sub> oxidized Ag/α-Al<sub>2</sub>O<sub>3</sub> (40% O<sub>2</sub>, 250 °C for 30 min post dehydration). (d) Spectra of products and reactants formed during 10% C<sub>2</sub><sup>-</sup> + 4% O<sub>2</sub>-TPSR over strongly oxidized Ag/α-Al<sub>2</sub>O<sub>3</sub>, (e, f) Spectra of products formed during C<sub>2</sub><sup>-</sup>-TPSR (5% C<sub>2</sub><sup>-</sup>, 50–500 °C, 10 °C/min) over (e) mildly O<sub>2</sub> oxidized Ag/α-Al<sub>2</sub>O<sub>3</sub> and (f) strongly O<sub>2</sub> oxidized Ag/α-Al<sub>2</sub>O<sub>3</sub>.

change in Figure 2a is shown in Figure S10. DFT-optimized molecular representations of the carbonate formation and CO<sub>2</sub> desorption are included in Figure S11.

**3.3. Temperature-Programmed Surface Reaction of Ethylene on Oxidized Ag Nanoparticles on α-Al<sub>2</sub>O<sub>3</sub>.** Variations in the surface oxygen species on/in the Ag surface during reaction with C<sub>2</sub><sup>-</sup> could be probed by *in situ* Raman spectroscopy. Accompanied with the monitoring of reaction products with mass spectroscopy, the selective oxygen species could be discerned, thus establishing fundamental understanding on the structure-performance relationship. The *in situ* SERS of Ag/α-Al<sub>2</sub>O<sub>3</sub> catalyst during C<sub>2</sub><sup>-</sup> + O<sub>2</sub>-TPSR, as well as C<sub>2</sub><sup>-</sup>-TPSR after mild oxidation and strong oxidation, are presented in Figure 4a–c, respectively. *In situ* Raman spectra of the Ag surface exhibit the presence of surface/subsurface Ag–O\* (300–315 and 615 cm<sup>-1</sup>),<sup>21</sup> dioxygen species in the surface troughs Ag–O<sub>2</sub>\* (715–718 cm<sup>-1</sup>),<sup>19</sup> and surface carbonates species (980–990 from Ag<sub>2</sub>CO<sub>3</sub> and 1057–1067 cm<sup>-1</sup> from Na<sub>2</sub>CO<sub>3</sub>)<sup>50,51</sup> The surface Ag–O<sub>2</sub>\* (815–820 cm<sup>-1</sup>) species are unique to the strong O<sub>2</sub> oxidation pretreatment (Figure 4a,c) that agrees with the recent observations for unsupported Ag powder.<sup>20,21</sup> The Na impurity, which is common for α-Al<sub>2</sub>O<sub>3</sub> supports, is also detected with HS-LEIS on oxidized Ag/α-Al<sub>2</sub>O<sub>3</sub> catalyst (Figure S12)<sup>52</sup> and accounts for the Na<sub>2</sub>CO<sub>3</sub> species. It is noted that the Ag signal increases with depth, suggesting that oxygen might concentrate on the surface (outermost 3 nm). Generally, it is observed the intensities of Raman bands associated with nearly all Ag–O<sub>x</sub> species during C<sub>2</sub><sup>-</sup> + O<sub>2</sub>-TPSR and C<sub>2</sub><sup>-</sup>-TPSR decrease with increasing reaction

temperature, suggesting their participation in reacting with ethylene. The evolution of the normalized intensity of each Raman band during TPSR in Figure 4a–c with respect to the stable CO<sub>3</sub><sup>2-</sup> species is plotted in Figure S13.

The product formation during C<sub>2</sub><sup>-</sup> + O<sub>2</sub>-TPSR and C<sub>2</sub><sup>-</sup>-TPSR are presented in Figure 4d–f. During C<sub>2</sub><sup>-</sup> + O<sub>2</sub>-TPSR over the strongly oxidized Ag/α-Al<sub>2</sub>O<sub>3</sub> (Figure 4d), the EO and CO<sub>2</sub> products formation light off at ~100 °C. The EO formation reaches its maximum at 202 °C, then continuously decreases while CO<sub>2</sub> production increases. The EO selectivity during the C<sub>2</sub><sup>-</sup> + O<sub>2</sub> TPSR from 100 to 300 °C is illustrated in Figure S14. The initial EO selectivity is around 50% and gradually diminishes to ~10% at maximum temperature, such observations show excellent agreement with the performance of unpromoted Ag catalysts reported in the literature.<sup>5</sup> C<sub>2</sub><sup>-</sup>-TPSR spectra from the mildly oxidized supported Ag/α-Al<sub>2</sub>O<sub>3</sub> catalysts yield only CO<sub>2</sub> as the carbon-containing reaction product (*T*<sub>p</sub> = 100–110 °C) (Figure 4e). Without the continuous O<sub>2(g)</sub> feed, only the strongly oxidized Ag/α-Al<sub>2</sub>O<sub>3</sub> catalyst shows the formation of both EO (*T*<sub>p</sub> = 166 and 195 °C) and CO<sub>2</sub> (*T*<sub>p</sub> = 166 and 195 °C) with the first peak smaller than the second peak (Figure 4f). The formation of selective oxidation products in the C<sub>2</sub><sup>-</sup>-TPSR spectra is in accordance with the decreasing intensity of the Raman band from surface Ag<sub>4</sub>-O<sub>2</sub>\* (815–820 cm<sup>-1</sup>) during C<sub>2</sub><sup>-</sup>-TPSR (Figure 4c). The shift of the *T*<sub>p</sub> value for CO<sub>2</sub> formation from 100 to 166/195 °C with the increasing extent of preoxidation suggests that the strength of the Ag–O bond increases for the strongly oxidizing pretreatment (also reflected by the shift of the O<sub>2</sub>-TPD peak from 250 to 291 °C with the extent of

preoxidation, Figure S9). The simultaneous production of EO and CO<sub>2</sub> from the strongly oxidized Ag surface under both C<sub>2</sub><sup>=</sup> + O<sub>2</sub>-TPSR ( $T_{\text{ligthoff}} = 100\text{ }^{\circ}\text{C}$ ) and C<sub>2</sub><sup>=</sup>-TPSR ( $T_p = 166$  and  $195\text{ }^{\circ}\text{C}$ ) suggests that both reaction products may originate from a common surface reaction intermediate. The EO selectivity during C<sub>2</sub><sup>=</sup>-TPSR from the strongly oxidized Ag catalyst is ~5%, which is significantly lower than the EO selectivity under C<sub>2</sub><sup>=</sup> + O<sub>2</sub>-TPSR conditions (~10–50%) and probably reflects the different gas phase and surface states of the catalysts without/with continuous feeding of O<sub>2</sub>, respectively. The absence of detectable molecular O<sub>2</sub> desorption during C<sub>2</sub><sup>=</sup>-TPSR reveals that surface O\* species hardly recombine and evolve as O<sub>2</sub> in the presence of ethylene. Interestingly, the CO<sub>2</sub> signal during C<sub>2</sub><sup>=</sup>-TPSR over the strongly oxidized Ag particles does not immediately go back to the baseline after the major CO<sub>2</sub> peaks and remains as a “tail” at higher temperatures (Figure 4f), which is also found in the previous literature.<sup>10,12</sup> Such behavior may reflect the slow reaction between C<sub>2</sub>H<sub>4</sub> and subsurface oxygen species that diffuse to the surface of Ag that reflects a Mars-van Krevelen (MvK) reaction mechanism, especially at higher temperatures. The MvK reaction mechanism cannot be the primary reaction mechanism of EO formation under steady-state ethylene oxidation reaction conditions since the EO selectivity during C<sub>2</sub><sup>=</sup>-TPSR is significantly lower than the 50% typically observed under steady state. Considering the *operando* Raman-MS investigation during C<sup>18</sup>O<sub>2</sub> exchange (Figure 2a), the results agree well with the observations from Lamoth et al. that the mild surface oxygen capable of exchanging <sup>16</sup>O with C<sup>18</sup>O<sub>2</sub> is selective toward EO formation while the strongly bonded lattice O\* is inaccessible to C<sup>18</sup>O<sub>2</sub> exchange and unselective in ethylene oxidation.<sup>44</sup> Trace amounts of H<sub>2</sub>O produced in the C<sub>2</sub><sup>=</sup>-TPSR experiment are hard to detect because of the adsorption of moisture on the α-Al<sub>2</sub>O<sub>3</sub> support and the tubing line from the fixed-bed reactor to the MS. The production of CO could also not be monitored because of its overlap with the strong MS signal from C<sub>2</sub>H<sub>4</sub> ( $m/z = 28$ ), but previous studies (Figure S1) have shown that CO is not a reaction product for ethylene oxidation by Ag.<sup>11,53</sup> The extent of preoxidation of the Ag nanoparticles could be varied by employing different pretreatments as shown in Figure S9. Desorption of O<sub>2</sub> from the pre-oxidized Ag surfaces initiates at 200 °C and the peak temperature, as well as the amount of O<sub>2</sub> desorbed from the Ag surface follows the order of strong O<sub>2</sub> oxidation > temperature-programmed ethylene oxidation > mild O<sub>2</sub> oxidation. In concert with the above findings, near ambient pressure-X-ray photoelectron spectroscopy (NAP-XPS) of Ag 3d spectra (Figure S15a) also exhibits that the surface of the Ag particles is sufficiently oxidized upon strong oxidation treatment and subsequently reduced after C<sub>2</sub><sup>=</sup>-TPSR. However, the predominate contribution to the O 1s spectra (Figure S15b) is an oxygen signal from the Al<sub>2</sub>O<sub>3</sub> support instead of the thin oxide layer of Ag, thus creating considerable challenge to draw relation to previous XPS studies with unsupported Ag.<sup>54,55</sup>

Comparison of the C<sub>2</sub><sup>=</sup>-TPSR spectra from the mildly and strongly O<sub>2</sub> oxidized supported Ag/α-Al<sub>2</sub>O<sub>3</sub> catalysts demonstrates that mild oxidation of Ag is insufficient to form an oxidized surface capable of EO formation (as reported by Campbell et al.).<sup>9</sup> For studies with Ag single crystals under UHV conditions, the adsorbed ethylene was not found to react with surface atomic oxygen species on the Ag(110) surface.<sup>53</sup> The observations of formation of EO and CO<sub>2</sub> from strongly

oxidized Ag single crystals,<sup>11</sup> Ag foils,<sup>10</sup> and supported Ag/Al<sub>2</sub>O<sub>3</sub> catalysts<sup>12</sup> demonstrate that Ag must be sufficiently oxidized to be able to perform ethylene epoxidation. The lower  $T_p$  value for reaction products from the mildly oxidized catalyst versus the strongly oxidized catalyst further reveals that weakly bound oxygen species readily participate in the ethylene combustion reaction. The above observations resolve the puzzles of the different Ag-catalytic C<sub>2</sub><sup>=</sup>-TPR/TPSR results reported in the literature over the years and show that the contradictory results are mainly related to the different types of oxygen species caused by the extent of oxidation of the Ag catalysts.

**3.4. Adsorption and Reaction of Ethylene with Strongly Oxidized Supported Ag/α-Al<sub>2</sub>O<sub>3</sub> Catalyst (Pretreated with Molecular O<sub>2(g)</sub>).** The adsorption and reaction/desorption of ethylene over a strongly oxidized supported Ag/α-Al<sub>2</sub>O<sub>3</sub> catalyst was monitored with *in situ* Raman spectroscopy and presented in Figure 5. The strongly

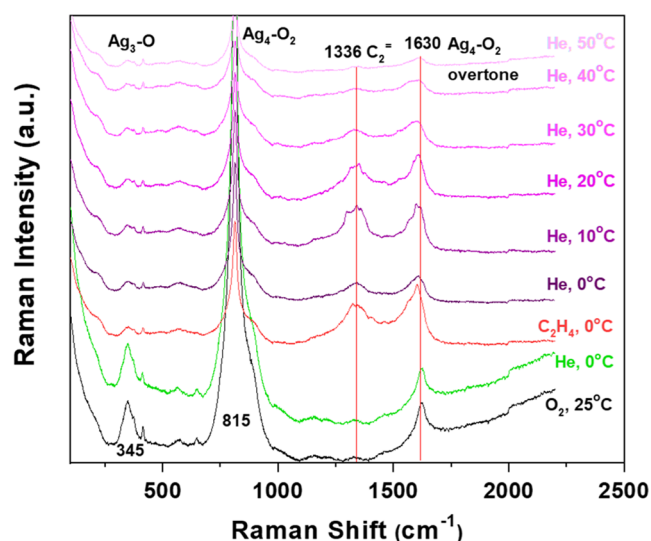


**Figure 5.** *In situ* Raman spectra of low temperature adsorption of ethylene on a dehydrated and oxidized Ag surface (10%O<sub>2</sub>/Ar, 300 °C, 1 h) of the supported Ag/α-Al<sub>2</sub>O<sub>3</sub> catalyst.

oxidized catalyst exhibited vibrations at ~345 cm<sup>-1</sup> (Ag–O\*), 815 cm<sup>-1</sup> (surface Ag–O<sub>2</sub>\*), and the corresponding overtone at ~1630 cm<sup>-1</sup> (815 cm<sup>-1</sup> × 2 = 1630 cm<sup>-1</sup>). Exposure to ethylene at 0 °C resulted in a new Raman band at ~1336 cm<sup>-1</sup> corresponding to the C=C vibrations of adsorbed molecular CH<sub>2</sub>=CH<sub>2</sub>.<sup>56</sup> Heating the catalyst from 0 to 50 °C led to the disappearance of the adsorbed ethylene band and significantly decreased the intensity of the Raman bands from the Ag–O\* and Ag–O<sub>2</sub>\* vibrations. These *in situ* Raman spectra reveal that ethylene does adsorb on an oxidized Ag surface and that ethylene can desorb and/or react with Ag–O\* and surface Ag–O<sub>2</sub>\* species at rather mild temperatures. Owing to the fact that O<sub>2</sub> desorption initiates at ~190 °C from the oxidized Ag surface (Figure S9), which is much higher than the temperature range where the intensity of the Raman bands from Ag–O\* decrease and surface Ag<sub>x</sub>–O<sub>2</sub>\* species are observed in Figure 5, it is concluded that the decreased concentration of adsorbed oxygen species is due to consumption by the ethylene oxidation reaction. The fact that ethylene is adsorbed on an oxidized Ag surface demonstrates that ethylene oxidation over an oxidized

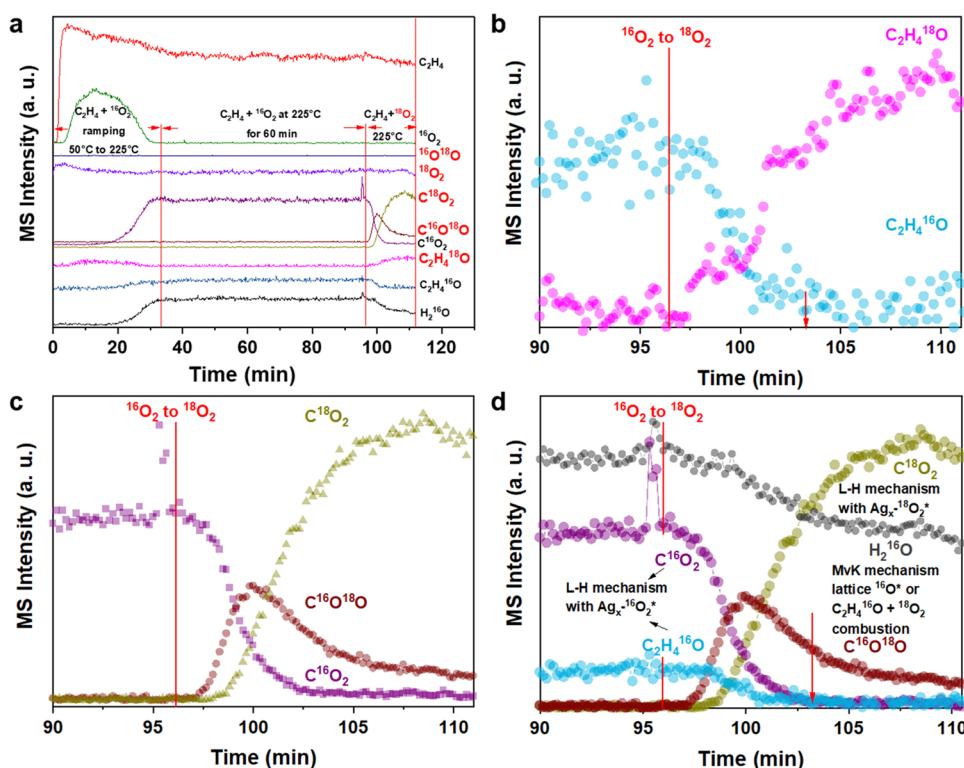


**Figure 6.**  $C_2H_4 + {}^{16}O_2 \rightarrow {}^{18}O_2$  SSITKA studies over the supported  $Ag/\alpha-Al_2O_3$  catalyst during steady-state ethylene oxidation (flow conditions: 12 000 ppm of  $C_2H_4$ , 3000 ppm of  $O_2$  and balance with Ar). The supported  $Ag/\alpha-Al_2O_3$  catalyst was initially dehydrated and pre-oxidized with  ${}^{16}O_2$  at 300 °C and then conditioned in the ethylene oxidation reaction environment with flowing  $C_2H_4-{}^{16}O_2$  by ramping the temperature from 50 to 225 °C and holding the catalyst at 225 °C for an additional 50 min (a) Overview of all reactants and products tracked with MS during the isotopic switch experiment. (b) Zoomed in time-resolved EO product signals during the isotope switch period. (c) Zoomed in time-resolved  $CO_2$  product signals during the isotope switch period. (d) Zoomed in time-resolved  ${}^{16}O$ -containing products and  $C^{18}O_2$  signals during the isotope switch period. The  $H_2{}^{18}O$  product could not be monitored because of its overlap with the strong MS signal from  $Ar^+$  ( $m/z = 20$ ). The spike in the signals at  $\sim 95$  min was caused by switching of the valves that controlled the flows of  ${}^{16}O_2/Ar$  and  ${}^{18}O_2/Ar$ .

supported  $Ag/\alpha-Al_2O_3$  catalyst does not proceed via the E-R (L-R) mechanism that assumes that ethylene is never adsorbed on the oxidized Ag surface during ethylene oxidation as sometimes proposed. In Table S2, DFT calculations also provide adsorption energies of ethylene on various Ag surfaces, showing that the oxidized Ag catalyst surface ( $p(4 \times 4)-O-Ag(111)$ ) exhibited ethylene binding energies that are more stable relative to the metallic Ag surfaces that further support the notion of an adsorbed ethylene in the reaction mechanism. A summary of the assignments of all species observed during *in situ/operando* Raman spectroscopy investigations by DFT calculations is given in Table 1.

**3.5. Steady-State Isotopic Transient Kinetic Analysis (SSITKA) during Ethylene Oxidation with  ${}^{16}O_2-{}^{18}O_2$  Switch.** Additional insights about the participation of molecular  $O_{2(g)}$  in the ethylene oxidation reaction by the supported  $Ag/\alpha-Al_2O_3$  catalyst were probed by performing ethylene oxidation with a SSITKA isotopic switch of the  ${}^{16}O_{2(g)} \rightarrow {}^{18}O_{2(g)}$  experiment as shown in Figure 6. The catalyst was pre-oxidized and then conditioned under the ethylene oxidation reaction conditions (see caption of Figure 6 for details). After conditioning the catalyst and reaching steady-state  $C_2H_4 + O_2$  reaction conditions, the  ${}^{16}O_{2(g)} \rightarrow {}^{18}O_{2(g)}$  isotopic switch was performed. The isotopic switch decreased the MS signals for the  $C_2H_4{}^{16}O$  and  $C^{16}O_2$  reaction products and within minutes these products were no longer being formed after  $t = 103$  min (Figure 6a–6c). Concurrently, the MS signals for the  ${}^{18}O$ -isotopically labeled products

( $C_2H_4{}^{18}O$  and  $C^{18}O^{16}O/C^{18}O_2$ ) simultaneously increased, with  $C_2H_4{}^{18}O$  and  $C^{18}O_2$  becoming the dominant products within minutes (Figure 6a–6c). After the isotopic switch, the production of  ${}^{16}O$ -containing and  ${}^{18}O$ -containing products (e.g.,  $C_2H_4{}^{16}O$  and  $C_2H_4{}^{18}O$  isotopes) reflected the relative populations of  ${}^{16}O$  and  ${}^{18}O$  species from the catalyst. Formation of  $C_2H_4{}^{16}O$  ceased even though formation of  $C^{16}O^{18}O$  persisted, which indicates that  $C_2H_4{}^{16}O$  production best proceeds in the presence of gas phase molecular  ${}^{16}O_2$  supplying the surface oxygen. This observation indicates that ethylene oxidation to EO mostly occurs during steady-state reaction in the presence of gas phase molecular  $O_2$  and thus proceeds via the L–H reaction mechanism. The loss of  $C^{16}O_2$  and formation of  $C^{18}O_2$  within minutes during the isotopic switch indicates that the ethylene oxidation to the  $CO_2$  reaction also primarily proceeds via the L–H reaction mechanism (Figure 6d). Additionally, the MS signal for the scrambled  ${}^{16}O^{18}O$  isotope was not detected after the  ${}^{16}O_{2(g)} \rightarrow {}^{18}O_{2(g)}$  isotopic switch (Figure S16) indicates that  $O_{2(g)}$  adsorption on Ag is an irreversible kinetic step during the ethylene oxidation reaction. Reaction pathway exploration via DFT reveals that the activation barrier for recombination of the  $O^*$  species to form the  $O_2^*$  was on the order of 1.00 eV, further underlining the unlikelihood of observing the mixed isotope dioxygen species. The production of  $C^{16}O^{18}O$  is a consequence of two concurrent events: ethylene combustion with surface  ${}^{16}O^*$ - and  ${}^{18}O^*$  species and combustion of  $C_2H_4{}^{16}O$  with  ${}^{18}O_2$ . As illustrated in Figure S17, the EO +  $O_2$ -

TPSR spectra over a reaction-treated Ag/ $\alpha$ -Al<sub>2</sub>O<sub>3</sub> catalyst show that ~8% EO is combusted at 225 °C. The C<sub>2</sub><sup>-</sup>-TPSR studies with a pre-oxidized Ag surface containing <sup>16</sup>O and <sup>18</sup>O (Figure S1c) indicate that C<sup>16</sup>O<sub>2</sub> and C<sup>18</sup>O<sub>2</sub> are produced at the same temperature (~350–420 K). Thus, there is only a minor kinetic oxygen isotopic effect for ethylene combustion. The continued presence of residual C<sup>16</sup>O<sup>18</sup>O at longer times indicates that the MvK reaction mechanism is also operating for ethylene combustion via subsurface or bulk lattice <sup>16</sup>O that diffuses to the surface. As indicated in Table S3, during the transient isotopic switch of <sup>16</sup>O<sub>2(g)</sub> → <sup>18</sup>O<sub>2(g)</sub>, C<sup>16</sup>O<sup>18</sup>O produced from the lattice \*<sup>16</sup>O contributes to ~16% of the total CO<sub>2</sub> formation. Hence, the production of CO<sub>2</sub> via the lattice MvK reaction mechanism is estimated to contribute ~16% of the overall combustion pathway.

#### 4. CONCLUSIONS

This study demonstrates that the  $\alpha$ -Al<sub>2</sub>O<sub>3</sub>-supported Ag nanoparticles possess an abundant amount of oxygen species during the ethylene oxidation reaction. This oxygen is plausibly well distributed near the surface region but could possess regions of partially oxidized Ag interspersed with metallic domains. Boltzmann distribution of stable surfaces constructed from DFT calculations suggests p(4 × 4)-O-Ag(111) more thermodynamically stable than metallic Ag(111) under typical ethylene oxidation environment, in support of the surface being populated largely by near-surface oxygen along with the presence of metallic domains. Combined *in situ* SERS and computational efforts illustrate multiple oxygen species (surface/lattice Ag<sub>x</sub>-O\* and surface Ag<sub>x</sub>-O<sub>2</sub>\*) are present on/in the Ag nanoparticles and dynamically vary with environmental conditions. Mildly O<sub>2</sub> oxidized Ag nanoparticles primarily contain Ag<sub>x</sub>-O\* (314 and 614 cm<sup>-1</sup>) species that only yield CO<sub>2</sub> during ethylene oxidation. Strongly O<sub>2</sub> oxidized Ag particles also contain chemisorbed surface dioxygen Ag<sub>4</sub>-O<sub>2</sub>\* species (815 cm<sup>-1</sup>) that yield both EO and CO<sub>2</sub> during C<sub>2</sub><sup>-</sup>-TPSR and C<sub>2</sub><sup>-</sup> + O<sub>2</sub>-TPSR experiments. These observations reconcile the differing C<sub>2</sub><sup>-</sup>-TPR results with pre-oxidized Ag catalysts reported in the literature since EO formation requires the presence of a more substantially oxidized Ag surface that was not achieved in many of the studies at low O<sub>2(g)</sub> pressures. The selective oxidation of ethylene to EO proceeds by the L-H reaction mechanism, and ethylene combustion proceeds via both L-H (predominant) and MvK (minor) reaction mechanisms. Ethylene oxidation by Ag does not proceed via the Eley (Langmuir)-Rideal reaction mechanism since ethylene adsorbs and reacts with the oxygen species present on/in the oxidized Ag nanoparticles.

#### ■ ASSOCIATED CONTENT

##### SI Supporting Information

The Supporting Information is available free of charge at <https://pubs.acs.org/doi/10.1021/acscatal.3c04361>.

Experimental materials and characterization methods; supporting figures and tables for characterization and DFT calculations including HAADF-STEM-EDS images; molecular structures; species binding energies and vibrational frequencies; HS-LEIS measurements; *in situ* XRD and UV-vis; calculated <sup>18</sup>O-<sup>16</sup>O isotope shift, *etc* (PDF)

#### ■ AUTHOR INFORMATION

##### Corresponding Authors

Eric A. Stach – Department of Materials Science and Engineering, University of Pennsylvania, Philadelphia, Pennsylvania 19104, United States; [orcid.org/0000-0002-3366-2153](https://orcid.org/0000-0002-3366-2153); Email: [stach@seas.upenn.edu](mailto:stach@seas.upenn.edu)

Srinivas Rangarajan – Computational Catalysis and Materials Design Group, Department of Chemical and Biomolecular Engineering, Lehigh University, Bethlehem, Pennsylvania 18015, United States; [orcid.org/0000-0002-6777-9421](https://orcid.org/0000-0002-6777-9421); Email: [srr516@lehigh.edu](mailto:srr516@lehigh.edu)

Israel E. Wachs – Operando Molecular Spectroscopy and Catalysis Laboratory, Department of Chemical and Biomolecular Engineering, Lehigh University, Bethlehem, Pennsylvania 18015, United States; [orcid.org/0000-0001-5282-128X](https://orcid.org/0000-0001-5282-128X); Email: [iew0@lehigh.edu](mailto:iew0@lehigh.edu)

##### Authors

Tiancheng Pu – Operando Molecular Spectroscopy and Catalysis Laboratory, Department of Chemical and Biomolecular Engineering, Lehigh University, Bethlehem, Pennsylvania 18015, United States; [orcid.org/0000-0002-4775-4294](https://orcid.org/0000-0002-4775-4294)

Adhika Setiawan – Computational Catalysis and Materials Design Group, Department of Chemical and Biomolecular Engineering, Lehigh University, Bethlehem, Pennsylvania 18015, United States; [orcid.org/0000-0001-7908-6473](https://orcid.org/0000-0001-7908-6473)

Alexandre C. Foucher – Department of Materials Science and Engineering, University of Pennsylvania, Philadelphia, Pennsylvania 19104, United States

Mingyu Guo – Operando Molecular Spectroscopy and Catalysis Laboratory, Department of Chemical and Biomolecular Engineering, Lehigh University, Bethlehem, Pennsylvania 18015, United States

Jih-Mirn Jehng – Operando Molecular Spectroscopy and Catalysis Laboratory, Department of Chemical and Biomolecular Engineering, Lehigh University, Bethlehem, Pennsylvania 18015, United States

Minghui Zhu – State Key Laboratory of Chemical Engineering, East China University of Science and Technology, Shanghai 200237, China; [orcid.org/0000-0003-1593-9320](https://orcid.org/0000-0003-1593-9320)

Michael E. Ford – Operando Molecular Spectroscopy and Catalysis Laboratory, Department of Chemical and Biomolecular Engineering, Lehigh University, Bethlehem, Pennsylvania 18015, United States; [orcid.org/0000-0002-0403-801X](https://orcid.org/0000-0002-0403-801X)

Complete contact information is available at: <https://pubs.acs.org/10.1021/acscatal.3c04361>

##### Notes

The authors declare no competing financial interest.

#### ■ ACKNOWLEDGMENTS

The research at Lehigh University was financially supported by the NSF GOALI grant (#1804104). The assistance of Dr. Henry Luftman with the HS-LEIS measurements is gratefully acknowledged. A.C.F. acknowledges support from the Vagelos Institute of Energy Science and Technology at the University of Pennsylvania. A portion of the computational aspects of this work were conducted on Lehigh University's research computing infrastructure built with partial support from NSF

(#2019035). This work also used Stampede2 at TACC, and Expanse at SDSC through allocation CTS170035 from the Advanced Cyberinfrastructure Coordination Ecosystem: Services & Support (ACCESS) program, which is supported by National Science Foundation grants (#2138259, #2138286, #2138307, #2137603, and #2138296).

## REFERENCES

- (1) Rebsdat, S.; Mayer, D. Ethylene Oxide *Ullmann's Encycl. Ind. Chem.* 2003.
- (2) ReportLinker. Global Ethylene Oxide (EO) Industry *Glob. Ind. Anal.* 2021.
- (3) Linic, S.; Barteau, M. A. Formation of a Stable Surface Oxametallacycle That Produces Ethylene Oxide. *J. Am. Chem. Soc.* **2002**, *124*, 310–317.
- (4) Özbek, M. O.; van Santen, R. A. The Mechanism of Ethylene Epoxidation Catalysis. *Catal. Lett.* **2013**, *143*, 131–141.
- (5) Pu, T.; Tian, H.; Ford, M. E.; Rangarajan, S.; Wachs, I. E. Overview of Selective Oxidation of Ethylene to Ethylene Oxide by Ag Catalysts. *ACS Catal.* **2019**, *9*, 10727–10750.
- (6) Diao, W.; Digiulio, C. D.; Schaal, M. T.; Ma, S.; Monnier, J. R. An Investigation on the Role of Re as a Promoter in Ag-Cs-Re/ $\alpha$ -Al<sub>2</sub>O<sub>3</sub> High-Selectivity, Ethylene Epoxidation Catalysts. *J. Catal.* **2015**, *322*, 14–23.
- (7) Ghanta, M.; Subramaniam, B. Development of a Sustainable and Economically Viable Process for Making Ethylene Oxide: A Case Study. In *Encyclopedia of Sustainable Technologies*; Elsevier, 2017; Vol. 1, pp 373–385.
- (8) Barteau, M. A.; Madix, R. J. Low Pressure Oxidation of Ethylene on Ag(110): Possible Experimental Complications. *Surf. Sci.* **1981**, *103*, L171–L178.
- (9) Campbell, C. T.; Paffett, M. T. Model Studies of Ethylene Epoxidation Catalyzed by the Ag(110) Surface. *Surf. Sci.* **1984**, *139*, 396–416.
- (10) Bukhtiyarov, V. I.; Prosvirin, I. P.; Kvon, R. I. Study of Reactivity of Oxygen States Adsorbed at a Silver Surface towards C<sub>2</sub>H<sub>4</sub> by XPS, TPD and TPR. *Surf. Sci.* **1994**, *320*, L47–L50.
- (11) Grant, R. B.; Lambert, R. M. A Single Crystal Study of the Silver-Catalyzed Selective Oxidation and Total Oxidation of Ethylene. *J. Catal.* **1985**, *92*, 364–375.
- (12) Atkins, M.; Couves, J.; Hague, M.; Sakakini, B. H.; Waugh, K. C. On the Role of Cs, Cl and Subsurface O in Promoting Selectivity in Ag/ $\alpha$ -Al<sub>2</sub>O<sub>3</sub> Catalyzed Oxidation of Ethene to Ethene Epoxide. *J. Catal.* **2005**, *235*, 103–113.
- (13) Waugh, K. C.; Hague, M. The Detailed Kinetics and Mechanism of Ethylene Epoxidation on an Oxidised Ag/ $\alpha$ -Al<sub>2</sub>O<sub>3</sub> Catalyst. *Catal. Today* **2010**, *157*, 44–48.
- (14) Ozbek, M. O.; Onal, I.; Van Santen, R. A. Effect of Surface and Oxygen Coverage on Ethylene Epoxidation. *Top. Catal.* **2012**, *55*, 710–717.
- (15) Fellah, M. F.; Van Santen, R. A.; Onal, I. Epoxidation of Ethylene by Silver Oxide (Ag<sub>2</sub>O) Cluster: A Density Functional Theory Study. *Catal. Lett.* **2011**, *141*, 762–771.
- (16) Pu, T.; Jehng, J.-M.; Setiawan, A.; Mosevitzky Lis, B.; Ford, M. E.; Rangarajan, S.; Wachs, I. E. Resolving the Oxygen Species on Ozone Activated AgAu Alloy Catalysts for Oxidative Methanol Coupling. *J. Phys. Chem. C* **2022**, *126*, 21568–21575.
- (17) Pettenkofer, C.; Pockrand, I.; Otto, A. Surface Enhanced Raman Spectra of Oxygen Adsorbed on Silver. *Surf. Sci.* **1983**, *135*, 52–64.
- (18) Pettinger, B.; Bao, X.; Wilcock, I.; Muhler, M.; Schlögl, R.; Ertl, G. Thermal Decomposition of Silver Oxide Monitored by Raman Spectroscopy: From Ago Units to Oxygen Atoms Chemisorbed on the Silver Surface. *Angew. Chem., Int. Ed. Engl.* **1994**, *33*, 85–86, DOI: 10.1002/anie.199400851.
- (19) Tang, Z.; Chen, T.; Liu, K.; Du, H.; Podkolzin, S. G. Atomic, Molecular and Hybrid Oxygen Structures on Silver. *Langmuir* **2021**, *37*, 11603–11610.
- (20) Pu, T.; Setiawan, A.; Mosevitzky Lis, B.; Zhu, M.; Ford, M. E.; Rangarajan, S.; Wachs, I. E. Nature and Reactivity of Oxygen Species on/in Silver Catalysts during Ethylene Oxidation. *ACS Catal.* **2022**, *12*, 4375–4381.
- (21) Liu, C.; Wijewardena, D. P.; Sviripa, A.; Sampath, A.; Flaherty, D. W.; Paolucci, C. Computational and Experimental Insights into Reactive Forms of Oxygen Species on Dynamic Ag Surfaces under Ethylene Epoxidation Conditions. *J. Catal.* **2022**, *405*, 445–461.
- (22) Schmid, M.; Reicho, A.; Stierle, A.; Costina, I.; Klikovits, J.; Kostelnik, P.; Dubai, O.; Kresse, G.; Gustafson, J.; Lundgren, E.; Andersen, J. N.; Dosch, H.; Varga, P. Structure of Ag(111)-p(4 × 4)-O: No Silver Oxide. *Phys. Rev. Lett.* **2006**, *96*, No. 146102.
- (23) Schnadt, J.; Knudsen, J.; Hu, X. L.; Michaelides, A.; Vang, R. T.; Reuter, K.; Li, Z.; Lægsgaard, E.; Scheffler, M.; Besenbacher, F. Experimental and Theoretical Study of Oxygen Adsorption Structures on Ag(111). *Phys. Rev. B* **2009**, *80*, No. 075424.
- (24) Jones, T. E.; Rocha, T. C. R.; Knop-Gericke, A.; Stampfl, C.; Schlögl, R.; Piccinin, S. Thermodynamic and Spectroscopic Properties of Oxygen on Silver under an Oxygen Atmosphere. *Phys. Chem. Chem. Phys.* **2015**, *17*, 9288–9312.
- (25) Bukhtiyarov, V. I.; Hävecker, M.; Kaichev, V. V.; Knop-Gericke, A.; Mayer, R. W.; Schlögl, R. Atomic Oxygen Species on Silver: Photoelectron Spectroscopy and x-Ray Absorption Studies. *Phys. Rev. B* **2003**, *67*, No. 235422.
- (26) Petrov, L.; Eliyas, A.; Shopov, D. A Kinetic Model of Steady State Ethylene Epoxidation over a Supported Silver Catalyst. *Appl. Catal.* **1985**, *18*, 87–103.
- (27) Force, E. L.; Bell, A. T. The Relationship of Adsorbed Species Observed by Infrared Spectroscopy to the Mechanism of Ethylene Oxidation over Silver. *J. Catal.* **1975**, *40*, 356–371.
- (28) Liu, J.-X.; Lu, S.; Ann, S.-B.; Linic, S. Mechanisms of Ethylene Epoxidation over Silver from Machine Learning-Accelerated First-Principles Modeling and Microkinetic Simulations. *ACS Catal.* **2023**, *13*, 8955–8962.
- (29) Prins, R. Eley–Rideal, the Other Mechanism. *Top. Catal.* **2018**, *61*, 714–721.
- (30) Lafarga, D.; Al-Juaied, M. A.; Bondy, C. M.; Varma, A. Ethylene Epoxidation on Ag-Cs/ $\alpha$ -Al<sub>2</sub>O<sub>3</sub> Catalyst: Experimental Results and Strategy for Kinetic Parameter Determination. *Ind. Eng. Chem. Res.* **2000**, *39*, 2148–2156.
- (31) Park, D. Ethylene Epoxidation on a Silver Catalyst: Unsteady and Steady State Kinetics. *J. Catal.* **1987**, *105*, 81–94.
- (32) Ghazali, S.; Park, D. W.; Gau, G. Kinetics of Ethylene Epoxidation on a Silver Catalyst. *Appl. Catal.* **1983**, *6*, 195–208.
- (33) Özbek, M. O.; Van Santen, R. A. The Mechanism of Ethylene Epoxidation Catalysis. *Catal. Lett.* **2013**, *143*, 131–141.
- (34) Perdew, J. P.; Burke, K.; Ernzerhof, M. Generalized Gradient Approximation Made Simple. *Phys. Rev. Lett.* **1996**, *77*, 3865–3868.
- (35) Becke, A. D.; Johnson, E. R. Exchange-Hole Dipole Moment and the Dispersion Interaction. *J. Chem. Phys.* **2005**, *122*, No. 154104.
- (36) Steinmann, S. N.; Corminboeuf, C. Comprehensive Benchmarking of a Density-Dependent Dispersion Correction. *J. Chem. Theory Comput.* **2011**, *7*, 3567–3577.
- (37) Steinmann, S. N.; Corminboeuf, C. A Generalized-Gradient Approximation Exchange Hole Model for Dispersion Coefficients. *J. Chem. Phys.* **2011**, *134*, No. 044117.
- (38) Sun, J.; Ma, D.; Zhang, H.; Liu, X.; Han, X.; Bao, X.; Weinberg, G.; Pfänder, N.; Su, D. Toward Monodispersed Silver Nanoparticles with Unusual Thermal Stability. *J. Am. Chem. Soc.* **2006**, *128*, 15756–15764.
- (39) Van Hoof, A. J. F.; Pilot, I. A. W.; Friedrich, H.; Hensen, E. J. M. Reversible Restructuring of Silver Particles during Ethylene Epoxidation. *ACS Catal.* **2018**, *8*, 11794–11800.
- (40) van Hoof, A. J. F.; van der Poll, R. C. J.; Friedrich, H.; Hensen, E. J. M. Dynamics of Silver Particles during Ethylene Epoxidation. *Appl. Catal., B* **2020**, *272*, No. 118983.
- (41) Bogdanchikova, N.; Meunier, F. C.; Avalos-Borja, M.; Breen, J. P.; Pstryakov, A. On the Nature of the Silver Phases of Ag/Al<sub>2</sub>O<sub>3</sub>

Catalysts for Reactions Involving Nitric Oxide. *Appl. Catal., B* **2002**, *36*, 287–297, DOI: [10.1016/S0926-3373\(01\)00286-7](https://doi.org/10.1016/S0926-3373(01)00286-7).

(42) More, P. M.; Nguyen, D. L.; Dongare, M. K.; Umbarkar, S. B.; Nuns, N.; Girardon, J. S.; Dujardin, C.; Lancelot, C.; Mamede, A. S.; Granger, P. Rational Preparation of Ag and Au Bimetallic Catalysts for the Hydrocarbon-SCR of NOx: Sequential Deposition vs. Coprecipitation Method. *Appl. Catal., B* **2015**, *162*, 11–20.

(43) Backx, C.; De Groot, C. P. M.; Biloen, P.; Sachtler, W. M. H. Interaction of O<sub>2</sub>, CO<sub>2</sub>, CO, C<sub>2</sub>H<sub>4</sub> and C<sub>2</sub>H<sub>4</sub>O with Ag(110). *Surf. Sci.* **1983**, *128*, 81–103.

(44) Lamoth, M.; Jones, T.; Plodinec, M.; Machoke, A.; Wrabetz, S.; Krämer, M.; Karpov, A.; Rosowski, F.; Piccinin, S.; Schlögl, R.; Frei, E. Nanocatalysts Unravel the Selective State of Ag. *ChemCatChem* **2020**, *12*, 2977–2988.

(45) Bertole, C. J.; Mims, C. A. Dynamic Isotope Tracing: Role of Subsurface Oxygen in Ethylene Epoxidation on Silver. *J. Catal.* **1999**, *184*, 224–235.

(46) Hess, C. New Advances in Using Raman Spectroscopy for the Characterization of Catalysts and Catalytic Reactions. *Chem. Soc. Rev.* **2021**, *50*, 3519–3564.

(47) Campbell, C. T. Atomic and Molecular Oxygen Adsorption on Ag(111). *Surf. Sci.* **1985**, *157*, 43–60.

(48) Citri, O.; Baer, R.; Kosloff, R. The Role of Non Adiabatic Mechanisms in the Dissociation Dynamics of O<sub>2</sub> on Silver Surfaces. *Surf. Sci.* **1996**, *351*, 24–42.

(49) Goikoetxea, I.; Beltrán, J.; Meyer, J.; Juaristi, J. I.; Alducin, M.; Reuter, K. Non-Adiabatic Effects during the Dissociative Adsorption of O<sub>2</sub> at Ag(111)? A First-Principles Divide and Conquer Study. *New J. Phys.* **2012**, *14*, No. 013050.

(50) Kondarides, D. I.; Papatheodorou, G. N.; Vayenas, C. G.; Verykios, X. E. In Situ High Temperature SERS Study of Oxygen Adsorbed on Ag: Support and Electrochemical Promotion Effects. *Ber. Bunsengesellschaft Phys. Chem.* **1993**, *97*, 709–719, DOI: [10.1002/bbpc.19930970511](https://doi.org/10.1002/bbpc.19930970511).

(51) Martina, I.; Wiesinger, R.; Jembrih-Simbürger, D.; Schreiner, M. Micro-Raman characterisation of silver corrosion products: instrumental set up and reference database. *E-Preserv. Sci.* **2012**, *9*, 1–8.

(52) Phung, T. K.; Herrera, C.; Larrubia, M. Á.; García-Diéguez, M.; Finocchio, E.; Alemany, L. J.; Busca, G. Surface and Catalytic Properties of Some  $\gamma$ -Al<sub>2</sub>O<sub>3</sub> Powders. *Appl. Catal., A* **2014**, *483*, 41–51, DOI: [10.1016/j.apcata.2014.06.020](https://doi.org/10.1016/j.apcata.2014.06.020).

(53) Barteau, M. A.; Madix, R. J. Low Pressure Oxidation of Ethylene on Ag(110): Possible Experimental Complications. *Surf. Sci. Lett.* **1981**, *103* (2-3), L171–L178, DOI: [10.1016/0167-2584\(81\)90634-4](https://doi.org/10.1016/0167-2584(81)90634-4).

(54) Carbonio, E. A.; Rocha, T. C. R.; Klyushin, A. Y.; Piš, I.; Magnano, E.; Nappini, S.; Piccinin, S.; Knop-Gericke, A.; Schlögl, R.; Jones, T. E. Are Multiple Oxygen Species Selective in Ethylene Epoxidation on Silver? *Chem. Sci.* **2018**, *9*, 990–998.

(55) Rocha, T. C. R.; Hävecker, M.; Knop-Gericke, A.; Schlögl, R. Promoters in Heterogeneous Catalysis: The Role of Cl on Ethylene Epoxidation over Ag. *J. Catal.* **2014**, *312*, 12–16.

(56) Pockrand, I. Ethylene on Silver: Development of Surface Enhanced Raman Lines with Exposure. *Surf. Sci.* **1983**, *126*, 192–196.